Molecular Crystals and Liquid Crystals

ISSN: 1542-1406 (Print) 1563-5287 (Online) Journal homepage: http://www.tandfonline.com/loi/gmcl20

Observation of Beam Self-Induced Transition from Positive to Negative Optical Refraction in Nematic Liquid Crystals

Nina Kravets, Armando Piccardi, Alessandro Alberucci, Oleksandr Buchnev & Gaetano Assanto

To cite this article: Nina Kravets, Armando Piccardi, Alessandro Alberucci, Oleksandr Buchnev & Gaetano Assanto (2015) Observation of Beam Self-Induced Transition from Positive to Negative Optical Refraction in Nematic Liquid Crystals, Molecular Crystals and Liquid Crystals, 619:1, 28-34, DOI: 10.1080/15421406.2015.1088761

To link to this article: http://dx.doi.org/10.1080/15421406.2015.1088761

Published online: 23 Oct 2015.

Mol. Cryst. Liq. Cryst., Vol. 619: pp. 28–34, 2015

ISSN: 1542-1406 print/1563-5287 online
DOI: 10.1080/15421406.2015.1088761

Observation of Beam Self-Induced Transition from Positive to Negative Optical Refraction in Nematic Liquid Crystals

NINA KRAVETS,[1,*] ARMANDO PICCARDI,[1] ALESSANDRO ALBERUCCI,[1] OLEKSANDR BUCHNEV,[2] AND GAETANO ASSANTO[1,3]

[1]NooEL – Nonlinear Optics and Optoelectronics Lab, University "Roma Tre," Rome, Italy
[2]Zepler Institute, University of Southampton, Southampton, United Kingdom
[3]Optics Laboratory, Dept. of Physics, Tampere University of Technology, Tampere, Finland

We demonstrate that light refraction at a straight interface between an isotropic dielectric and a nematic liquid crystal can change from positive to negative depending on power. The phenomenon relies on the reorientational response and the all-optical rotation of the optic axis, causing in turn variations in walk-off and beam self-steering.

Keywords nematic liquid crystals; negative refraction; optical solitons; nematicons; self-steering; signal routing

1. Introduction

As well known, light traveling across the interface between two media with different refractive indices undergoes refraction, i.e., its ray trajectory changes in order to minimize the optical path according to the Fermat principle or, equivalently, in order to conserve momentum across the interface; both approaches lead to the Snell's law, which predicts an angular deviation ruled by the ratio between the two refractive indices [1].

In *natural* isotropic media and away from the absorption regions, light crossing an interface is positively refracted, that is, incident and refracted rays lie on opposite sides of the interface normal; in other words, the transverse velocity maintains its sign after crossing the interface. An opposite and counter-intuitive behavior is expected in the presence of a negative refractive index, as it may occur in materials simultaneously exhibiting a negative magnetic permeability and a negative dielectric susceptibility, the so called metamaterials [2]. The most striking consequence of a negative index is that the phase velocity (i.e., the wave vector) is reversed with respect to the group velocity (i.e., the Poynting vector). When optical waves cross an interface and travel from a positive to a negative index medium,

*Address correspondence to Nina Kravets, NooEL – Nonlinear Optics and Optoelectronics Lab, University "Roma Tre" 00146, Rome, Italy. E-mail: kravetsnin@gmail.com

Color versions of one or more of the figures in the article can be found online at www.tandfonline.com/gmcl.

Snell's law holds valid as it basically relies on Maxwell's equations. However the refracted ray has an angle of opposite sign with respect to the interface normal due to the negative index: light is negatively refracted as its transverse velocity changes sign during refraction [3]. Negative refraction is the most striking evidence of a negative refractive index [4–7]; it can also occur in hyperbolic media with just a negative effective permittivity [8–9].

Negative refraction, that is, incident and refracted light beams propagating in the same half-plane with respect to the interface normal, can be observed in anisotropic materials with a positive index, as well, provided the wave vector and the Poynting vector are non-parallel [9–11]. The latter condition is easily achievable e.g. in non-magnetic uniaxial media, where the energy flux of an extraordinarily polarized wavepacket can propagate at a finite angle, the walk-off δ, with the wave vector [1]. Note that, in positive index materials, the wave vector obeys normal refraction whereas the Poynting vector can undergo negative refraction.

Negative refraction in uniaxial media is enhanced as the optical anisotropy increases: for this reason, owing to their large birefringence, most nematic liquid crystals (NLCs) are ideal candidates for the investigation of negative refraction. Moreover, due to sensitivity of NLCs to external stimuli, the amount and the nature (positive or negative) of refraction can be tuned via an applied voltage, as the latter can induce rotation of the optic axis [12]. Bias-adjustable negative refraction in NLCs has been demonstrated both for plane [12] and self-confined waves [13].

In this work we show how light beams crossing an interface between air and NLCs can "switch" from positive to negative refraction by simply increasing the input power. The phenomenon stems from the reorientational nonlinearity: the light-induced torque rotates the optic axis (i.e. the NLC molecular director), affecting the beam propagation in two ways: i) forming a graded-index waveguide able to confine the beam itself into a profile-invariant spatial solitary wave [14]; ii) altering the beam trajectory (Poynting vector) by varying the birefringent walk-off [15].

2. Basic Mechanism

Let us consider a light beam propagating in air and impinging on an NLC planar cell at an angle β_{in} with respect to the normal at the input interface (axis z). The NLC cell is such that the director $\hat{\mathbf{n}}$ in the sample is uniformly parallel to the z axis in the absence of external excitations (Fig. 1a). We consider standard (positive) uniaxial NLCs. This configuration helps maximizing self-induced negative refraction, as clarified hereafter.

The NLC birefringence and uniaxial nature give rise to different refractive indices for plane waves with electric field polarized parallel ($n_{||}$) and normal ($n_{\perp}$) to the optic axis (director $\hat{\mathbf{n}}$), respectively. The extraordinary wave component perceives a refractive index n_e dependent on the propagation direction: $n_e(\theta) = (\cos^2\theta/n_{\perp}^2 + \sin^2\theta/n_{||}^2)^{-1/2}$, where θ is the angle between the wave vector $\mathbf{k}$ and $\hat{\mathbf{n}}$. Snell's law for the wave vector takes the form $\sin\beta_{in} = n_e(\theta)\cdot\sin\beta$, where β is the angle of refraction in the NLC. The signs of β_{in} and β are always the same, so positive refraction always takes place in terms of phase velocity (Fig. 1a). However, for the same polarization, the (extraordinary) Poynting vector $\mathbf{S}$ is tilted by the walk-off angle $\delta = \arctan\{\varepsilon_a \sin(2\theta)/[\varepsilon_a + 2n_{\perp}^2 + \varepsilon_a\cos(2\theta)]\}$ with respect to $\mathbf{k}$, with $\varepsilon_a = n_{||}^2 - n_{\perp}^2$ the optical anisotropy. In the linear case (i.e., low input power) the molecular orientation is not affected by light: since in positive uniaxials the Poynting vector always lies coplanar between the wave vector and the optic axis, light rays are positively refracted, regardless of the incidence angle (Fig. 1a). Conversely, in the

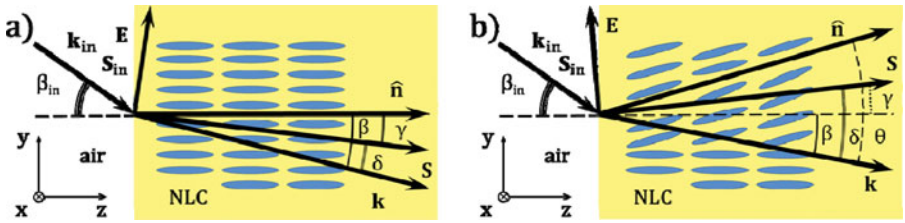

Figure 1. Sketch of beam self-induced negative refraction. a) Linear case of refraction at the interface between air and NLC. Refraction is positive due to the mutual alignment of beam wave vector and molecular director $\hat{\mathbf{n}}$ (long axis of the ellipses). b) Refraction in the highly nonlinear limit, i.e. in the presence of molecular reorientation. Refraction is positive in terms of wave vector **k** (phase velocity, angle β), but negative in terms of Poynting vector **S** (group velocity, angle γ). δ is the walk off and **E** the extraordinary-wave electric field. Input angle β_{in} is taken negative in this example.

nonlinear limit the light beam produces a substantial reorientation modifying θ and rotating the director towards positive (negative) y if $\beta_{in}<0$ ($\beta_{in}>0$), i.e., pushing the director away from the wave vector (see Fig. 1b) [16]. The induced variations on the angle θ between wave vector and director can increase the walk-off δ, eventually making it large enough to overcome the refraction angle β for small β_{in} (Fig. 1b): if $|\delta| > |\beta|$ both the refracted ray (parallel to the refracted Poynting vector **S)** and the incidence ray (parallel to the input wave vector $\mathbf{k}_{\text{in}}$) belong both to the half-plane $y > 0$, that is, the beam is subject to negative refraction.

From the discussion above it is clear that negative refraction can only be observed in a limited range of incidence angles β_{in}; the range widens as the anisotropy ε_a gets larger. In our experiments we used the standard NLC mixture E7, providing a maximum walk-off angle of about 7° in the near infrared. Simple calculations show that negative refraction in E7 can be observed at a wavelength of 1064 nm for $|\beta_{in}| < 12°$ [17].

3. Experimental Observation

We launched a TEM_{00} light beam at 1064 nm in the cell as sketched in Fig. 1; the input electric field was linearly polarized in yz to maximize the in-coupling to the extraordinary wave. A microscope objective (MO, Fig. 2a) allowed injecting the beam with a waist of about 8μm. The incidence angle β_{in} (with **k** and **E** in the yz plane) was impressed by

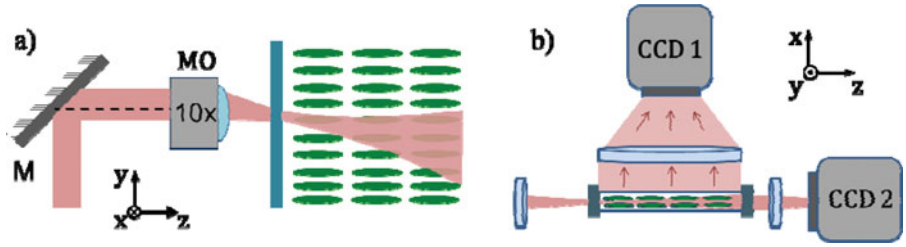

Figure 2. Details of the setup. (a) Beam coupling in the NLC cell and (b) acquisition of its intensity evolution images in the NLC. M indicates the (shiftable) mirror, MO the microscope objective; CCD1 and CCD2 are cameras imaging beam propagation in yz by collecting out-of-plane scattered light and beam output profile at the cell exit, respectively.

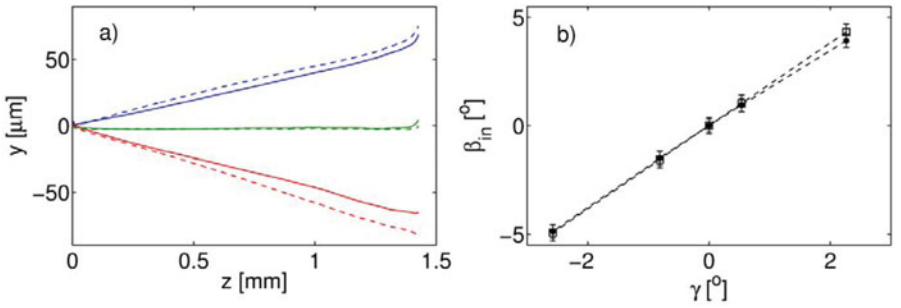

Figure 3. Evaluation of the beam incidence angle in *yz*. a) Low-power trajectories of extraordinary (solid) and ordinary (dashed) beams for various incidence angles. b) Incidence angle versus propagation angle of extraordinary beam, evaluated from Snell's law for ordinary polarization (dots) and from modified Snell's law to account for walk-off in the case of extraordinary polarization (squares). The trajectories in a) were found to correspond to incidence angles β_{in} of about -5° (red); 0° (green) and 5°(blue).

slightly translating the mirror (M) before the microscope objective (MO) and so offsetting the beam with respect to the MO symmetry axis (Fig. 2a). The beam evolution in the *yz* plane was acquired by collecting the scattered light via a CCD camera placed above the cell (CCD1, Fig. 2b). Another CCD camera (CCD2) placed after the cell was used to record the beam profile at the output. In the linear regime, the beam diffracted and propagated at an angle $\gamma = \beta - \delta$ with respect to *z*.

In order to accurately evaluate the incidence angle β_{in}, we measured the trajectories of both extraordinary (polarization in *yz*) and ordinary (polarization along *x*) wavepackets: normal incidence $\beta_{in} = 0$ corresponded to the maximum spatial overlap between the two wavepackets in the diffraction (linear) regime (Fig. 3a). Figure 3b shows good agreement between estimates from ordinary and extraordinary components. This procedure allowed us to associate a given mirror shift to the corresponding angle β_{in} at the cell input.

Then we investigated the propagation of an extraordinary beam as the input power was increased from 2 to 150 mW, for an incidence angle close to -9° (Fig. 4). As expected, at low powers the beam underwent standard refraction and diffraction in a uniform index medium. At input powers above 20mW the molecular reorientation was strong enough to induce self-trapping, i.e., diffractive spreading was compensated by self-focusing [14].

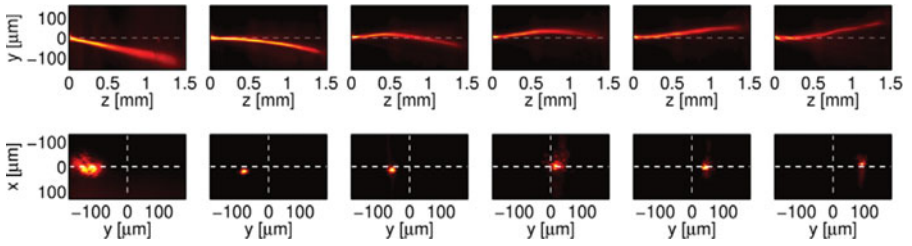

Figure 4. Observation of self-induced transition from positive to negative refraction. Top: beam evolution in *yz*: the dashed line is normal to the interface. Bottom: output beam profile in *xy* at the exit of the cell. Columns correspond to powers of 2; 20; 30; 40; 70 and 150 mW from left to right, respectively.

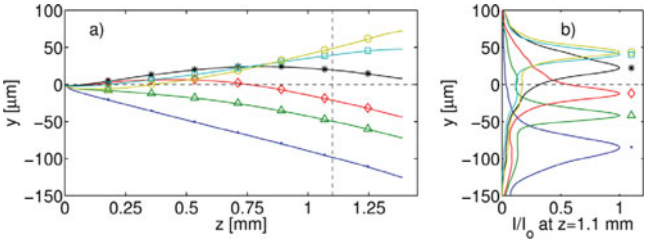

Figure 5. Power dependent walk-off and self-induced negative refraction. a) Beam trajectories for an incidence angle of about -9°. The beam power varied from 2 mW, (linear case, blue line with dots), via 20 mW (green with triangles), 30 mW (red with diamonds), 40 mW (black with asterisks), 70 mW (cyan with squares) to 150 mW (yellow with circles). b) Peak normalized yz beam intensity profiles in $z = 1.1$mm (vertical dashed line in a).

At the same time, the optic axis distribution was appreciably altered with respect to the unperturbed regime, yielding self-steering [15]. It is apparent in Fig. 4 that the beam trajectories are curved when reorientation takes place: the observed bending is caused by the unavoidable scattering losses, leading to power decay versus z, eventually weakening the nonlinear response and bringing the system back to its linear state [15].

The observed Poynting vector rotated toward the z-axis, as predicted in Fig. 1b; for powers close to 30 mW the self-trapped beam reached the point $y = 0$ close to the input interface (second panel from the left in Fig. 4). For further increases in power, the beam shifted to the half-plane $y > 0$, experiencing negative refraction (Fig. 4 and Fig. 5). The trajectories in Fig. 5 confirm that self-steering was due to nonlinear changes in walk-off, as the maximum slope of the beam path is about 7° with respect to z, corresponding to the maximum walk-off for the used NLC mixture and wavelength. For P = 150 mW the beam slope increases with propagation in contrary to evolution at lower power, when slope has maximum value in the beginning and decreases with propagation: this is consistent with the walk-off dependence on the angle θ between director and wave vector, with a maximum for $\theta \approx 45^\circ$.

The solitary paths versus power generally followed a similar trend when the incidence angles β_{in} varied between -9° and $+8^\circ$. The main difference was the walk-off required

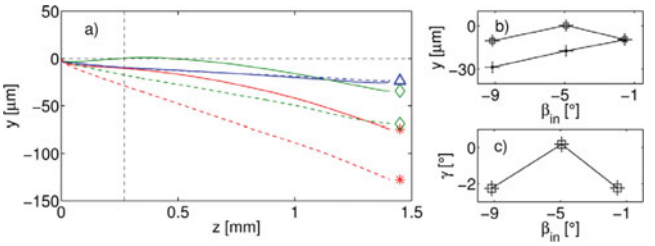

Figure 6. Role of the incidence angle. a) Beam trajectories in linear (2mW, dashed lines) and nonlinear (20mW, solid lines) regimes. Colors and markers refer to different incidence angles: red with asterisks $\beta_{in} = -9^\circ$, green with diamonds $\beta_{in} = -5^\circ$ and blue with triangles $\beta_{in} = -1^\circ$. b) y-position of beam center in $z = 0.27$mm (vertical dashed line in panel a) at 2 mW (dots) and 20 mW (squares) versus β_{in}. c) Angle γ calculated from the beam position in $z = [0; 0.27]$ mm for an input power of 20 mW.

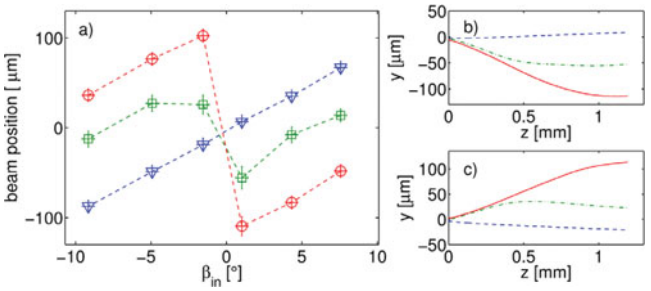

Figure 7. a) Transverse position of the beam across y, measured in $z = 1.1$ mm. Blue triangles refer to the linear case at 2 mW, green squares and red circles correspond to beam powers of 30 and 70 mW, respectively. b) Beam trajectories at powers 2 (dashed blue), 30 (dash-dotted green) and 100 mW (solid red) for incidence at about $+1^\circ$; c) same as in b) for incidence at about -1°.

to switch refraction from positive to negative and the corresponding input power. For example, Fig. 6 shows the acquired beam trajectories for an input power of 20 mW and three incidence angles: the nonlinear contribution to walk-off is large enough to overcome normal refraction for incidence angle about -5°, but refraction remains positive at β_{in} about -1°, thus showing a different behavior with respect to the simple model in Section 2. Such discrepancy can be readily explained noting that the nonlinearity, i.e., the light-induced changes in director orientation, drops off dramatically as the angle between the director and the electric field tends to 90° due to a vanishing torque (the orthogonality between field and optic axis involves the so called optical Fréedericksz transition with the appearance of a power threshold [14, 18, 19, 20]). Thus a 20mW beam entering the cell with a tilt of about -1° did not induce molecular reorientation large enough to provide a significant variation of its own trajectory. Nonetheless, all-optical reorientation sufficient to get negative refraction could be achieved by increasing the input power, even for an incidence angle of 1°. The results are summarized in Fig. 7, where the beam position along y, measured in $z = 1.1$ mm for three input powers, is plotted versus incidence angle β_{in}. For an input power of about 70 mW, negative refraction was obtained even for small angles. It can be seen that, as power increased, the beam position across y eventually went from negative to positive values. Thus, in the linear case and for negative incidence angles, the beam propagated in the half-plane $y < 0$; as power increased, all-optical reorientation deflected the beam towards the z axis (increasing y) until, when walk-off was large enough to overtake the wave vector refraction, the beams crossed the z axis and moved to positive y. The observed spatial dynamics with power at various incidence angles was in agreement with the predicted behavior for the E7 NLC mixture.

4. Conclusions

We experimentally demonstrated that optical refraction at the interface between air and nematic liquid crystals may change its nature from positive to negative thanks to the reorientational nonlinear response. Though power-controlled rotation of the optic axis, reorientation can change the walk-off angle and, in highly birefringence NLC, redirect the refracted Poynting vector in the same half-plane of the incident beam. The range of incidence angles allowing negative refraction is therefore dictated by the optical properties of nematic liquid crystals: the larger the optical anisotropy the wider the range. Owing to left-right symmetry with respect to normal incidence, the studied geometry permitted the

observation of power-driven negative refraction for both positive and negative incidence angles. Moreover, the geometry here employed yielded angular beam deflections as large as the maximum walk-off. Finally, these findings can be generalized to other types of anisotropic soft-matter where the nonlinearity acts on the orientation of the optic axis [21–22].

Acknowledgments

G.A. acknowledges the Academy of Finland for his Finnish Distinguished Professor project, grant no. 282858.

References

[1] Born, M., & Wolf, E. (1975). *Principles of optics*, Pergamon Press: New York.
[2] Veselago, V. G. (1968). *Soviet physics uspekhi*, *10*, 509–514.
[3] Shelby, R. A., Smith, D. R., & Schultz, S. (2001). *Science*, *292*, 77–79.
[4] Soukoulis, C. M., Linden S., & Wegener, M. (2007). *Science*, *315*, 47–49.
[5] Shalaev, V. M. *et al.* (2005). *Opt. Lett.*, *30*, 3356–3358.
[6] Xu, T., Agrawal, A., Abashin, M., Chau, K. J., & Lezec, H. J. (2013). *Nature*, *497*, 470–474.
[7] Yao, J. *et al.* (2008). *Science*, *321*, 930.
[8] Pawlik, G., Tarnowski, K., Walasik, W., Mitus, A. C., & Khoo, I. C. (2014). *Opt. Lett.*, *39*, 1744–1747.
[9] Luo, C., Johnson, S. G., Joannopoulos, J. D., & Pendry, J. B. (2002). *Phys. Rev. B*, *65*, 201104.
[10] Mackay, T. G., & Lakhtakia A. (2009). *Phys. Rev. B*, *79*, 235121.
[11] Zhang, Y., Fluegel, B., & Mascarenhas, A. (2003). *Phys. Rev. Lett.*, *91*, 157404.
[12] Peccianti, M., & Assanto, G. (2007). *Opt. Express*, *15*, 8021–8028.
[13] Pishnyak, O. P., & Lavrentovich, O. D. (2006). *Appl. Phys. Lett.*, *89*, 251103.
[14] Peccianti, M., & Assanto, G. (2012). *516*, 147–208.
[15] Piccardi, A., Alberucci, A., & Assanto, G. (2010). *Appl. Phys.Lett.*, *96*, 061105.
[16] de Gennes, P. G., & Prost, J. (1993). *The Physics of Liquid Crystals*, Oxford U. Press: London, UK. (b) Khoo, I. C. (1995). *Liquid Crystals: Physical Properties and Nonlinear Optical Phenomena*, Wiley: New York.
[17] Piccardi, A., Alberucci, A., Kravets, N., Buchnev, O., & Assanto, G. (2014). *Nat. Comm.*, *5*, 5533–5541.
[18] Freedericksz, V., & Zolina, V. (1933). *Trans. Faraday Soc.*, *29*, 919–930.
[19] Kravets, N., Piccardi, A., Alberucci, A., Buchnev, O., Kaczmarek, M., & Assanto, G. (2014). *Phys. Rev. Lett.*, *113*, 023901.
[20] Alberucci, A., Piccardi, A., Kravets, N., & Assanto, G. (2014). *Opt. Lett.*, *30*, 5830–5833.
[21] Lapine, M., Shadrivov, I. V., Powell, A. D., & Kivshar, Y. S. (2012). *Nat. Mater.*, *11*, 30–33.
[22] Shen, T.-Z., Song, S.-H., & Song, J.-K. (2014). *Nat. Mater.*, *13*, 394–399.